Faraday Discussions

Accepted Manuscript

This manuscript will be presented and discussed at a forthcoming Faraday Discussion meeting. All delegates can contribute to the discussion which will be included in the final volume.

Register now to attend! Full details of all upcoming meetings: http://rsc.li/fd-upcoming-meetings

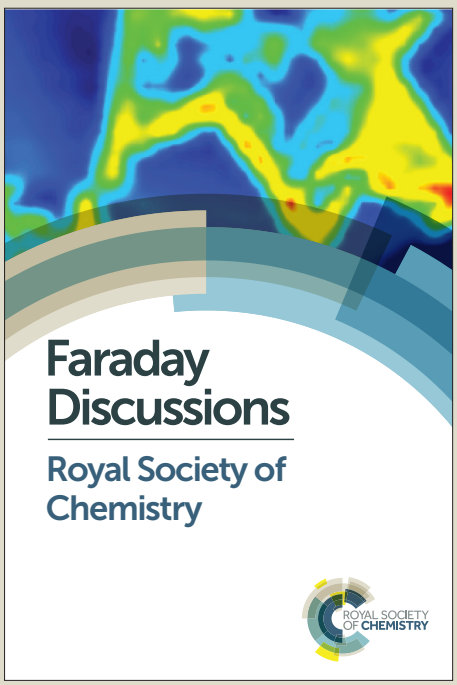

This is an *Accepted Manuscript*, which has been through the Royal Society of Chemistry peer review process and has been accepted for publication.

Accepted Manuscripts are published online shortly after acceptance, before technical editing, formatting and proof reading. Using this free service, authors can make their results available to the community, in citable form, before we publish the edited article. We will replace this *Accepted Manuscript* with the edited and formatted *Advance Article* as soon as it is available.

You can find more information about *Accepted Manuscripts* in the Information for Authors.

Please note that technical editing may introduce minor changes to the text and/or graphics, which may alter content. The journal's standard Terms & Conditions and the Ethical guidelines still apply. In no event shall the Royal Society of Chemistry be held responsible for any errors or omissions in this *Accepted Manuscript* or any consequences arising from the use of any information it contains.

ROYAL SOCIETY OF CHEMISTRY

www.rsc.org/faraday_d

Platinum and Platinum based nanoalloys synthesized by wet chemistry

Caroline Salzemann[1,2], Farid Kameche[1,2], Anh-Tu Ngo[1,2], Pascal Andreazza[3], Monica Calatayud[4,5,6] , Christophe Petit[1,2] *

1- Sorbonne Universités, UPMC Univ Paris 06, UMR 8233, MONARIS, 4 place Jussieu, F-75005, Paris, France

2- CNRS, UMR 8233, MONARIS, 4 place Jussieu, F-75005, Paris, France

3- Centre de Recherche sur la Matière Divisée, CRMD, Université d'Orléans, CNRS, 1bis rue de la Férollerie, F-45071, Orléans Cedex 2, France

4- Sorbonne Universités, UPMC Univ Paris 06, UMR 7616, Laboratoire de Chimie Théorique, F-75005, Paris, France

5- CNRS, UMR 7616, Laboratoire de Chimie Théorique, F-75005, Paris, France

6- Institut Universitaire de France.

Abstract

Platinum nanocrystals and its derivative with palladium and cobalt have a fundamental interest due to their large field of application in chemistry and physics. Their properties are strongly dependent on the shape and composition. However the chemical route is far to allow control both shape and composition. In this paper, we show both experimentally and theoretically the important role of the interaction of small adsorbed molecules on the shape but also on the control of composition. This has been studied by comparing the case of pure palladium and platinum nanocrystals and the case of PtPd and PtCo nanoalloys synthesized by the liquid-liquid phase transfer method.

A-Introduction

Inorganic nanocrystals, NCs, are widely studied and used in chemical, biological and physical devices. (*i.e.* in catalysis, magnetism, optics, etc.). Understanding their properties and exploring their applications are two major driving forces behind the synthesis of a large variety of nanomaterials. [1] It is now well known that the fine tuning of structural parameters such as the size, the shape and the bimetallic composition mainly controls these properties. Nowadays, platinum, palladium and their derivatives appear as good candidates for application in nanotechnology. [2] However these resources are scarce, hence it is necessary to develop new approaches to optimize their use in physical and chemical fields. In a sustainable approach, soft chemistry is well adapted to produce such metal nanoparticles and nanoalloys in large amount. However at the nanometer scale, as the properties are strongly dependent on the size and the surface state (raw or capped), it is crucial to develop methods where the polydispersity in size and composition is finely controlled. The proper designed wet chemistry synthesis, even in liquid isotropic solutions, offers a suitable way to produce metallic nanoparticles with designing composition and to control their shapes at the nanoscopic scale [3]. These processes are however quite complex as all the physical and chemical parameters could play an important role and up to date there is no clear answer to the control of both the particle nanomorphology and the particle composition. Indeed, many receipts exist without a general framework [2,4-6]. In order to give quantitative and qualitative response to these problems, we present here the synthesis of platinum and palladium nanocrystals and their nanoalloys Pt_xPd_{1-x} and Pt_xCo_{1-x}. On the one hand, *in situ* growth evolution of platinum and palladium nanocrystals under several chemical conditions, have been investigated by Small Angle X-ray Scattering. On the other hand TEM investigation of the crystallinity and the shape of the NC's has been performed. Density functional theory (DFT) calculations show the key role of hydrogen in the formation of cubic platinum shapes. These results illustrate both experimentally and theoretically, the primordial role of the capping agent and

of the dissolved gases issued either from air or as a by-product of the reaction, which may strongly influence the shape and the composition of NCs. In particular, platinum nanocubes are obtained only in the presence of an H_2 overpressure, due to a preferential adsorption on (100) facets compared to the (111) facets, whereas it is not possible to control the shape of palladium nanocrystals in similar condition due to a difference in the nature of interaction of H_2 with the palladium surfaces. In case of nanoalloys it demonstrates the important role of the kinetics of formation of the precursor to control the composition and its influence on the nanomorphology. The present work aims at shedding light in the complexity of the control of the nanomorphology and composition as it needs a fine tuning of the various physical-chemical parameters to establish a general framework of growth of metallic or bimetallic nanoparticles in solution.

B –Methods

B-1 Synthesis of metallic nanoparticles (figure 1):

Pt, Pd or Co nanocrystals and PtPd or CoPt nanoalloys are synthesized by phase transfer synthesis method presented by Brust et al. [7] Typically, it consists of metal ions transfer from an aqueous phase to an organic phase using an extractant molecule. The nanocrystals are obtained by chemical reduction.

B-1-1 Preparation of the metallic salt solution

Aqueous solutions of 3.3 10^{-2}M $PtCl_4$ (or $PdCl_2$ or $CoCl_2$) are prepared by dissolving the metallic salt in acid media to form the complexes H_2PtCl_6 (or H_2PdCl_4). This aqueous solution is then mixed with 1.9 x 10^{-2} M Tetrakis (Decyl) Ammonium Bromide (TDAB) dispersed in 80 cm^3 of toluene. To ensure maximum transfer of metal ions from the water phase to the organic phase, the transferring agent (TDAB) was present in large excess (corresponding to TDAB/ Metal = 3/1). The two phases mixture is vigorously stirred until all the metallic complexes are transferred into the organic phase (30 min). The colourless water phase is then discarded.

B-1-2 Chemical reduction of the metallic salt (Figure 1)

B-1-2-1 Procedure I: Reduction in presence of the capping agent

$1.2.10^{-2}$ mol of octylamine (C_8NH_2) used as Capping Agent (CA) is added under stirring to 40 cm^3 of the obtained organic solution containing the metallic complexes. A freshly prepared aqueous solution of $NaBH_4$ (10 cm^3, 1 $mol.L^{-1}$) is dropwise added under stirring, yielding to an emulsion. This induces the reduction of the metallic salt at the interface of the organic and aqueous phases. Both the reducing agent and the capping agent are added in large stoichiometric excess relative to the palladium/platinum/cobalt (for example $NaBH_4/Pt^{4+}$ =160:1 and CA/Pt = 96:1). The emulsion turns relatively fast from orange (in case of platinum) to dark brown. The reaction takes place for one night after what, the stirring is turned off and the organic phase, containing the metallic nanoparticles is collected and evaporated using a rotavapor. The black paste obtained is then washed with 40 cm^3 of ethanol. Then, the turbid solution is centrifuged and the supernatant is discarded. This operation is repeated twice. After the last centrifugation, the precipitate is redispersed in 4 cm^3 of toluene. The final solution contains the coated C_8NH_2-nanoparticles in toluene.

B-1-2-2 Procedure II: Reduction followed by the addition of capping agent.

In this case, the freshly prepared aqueous solution of $NaBH_4$ (10 cm^3, 1 $mol.L^{-1}$) is dropwise added under stirring to 20 cm^3 of the organic solution containing the metallic complexes. The reduction occurs in the emulsion phase, at the interface of the organic and aqueous phases, which results in a color change from orange to dark brown. After 60 minutes (ripening time τ_{rip}), 1.2 10^{-2} mol of octylamine (C_8NH_2) capping agent is then added. The chemical bath is kept under stirring for one night, then the nanocrystals are extracted following the procedure described above. The final solution contains the coated C_8NH_2-nanoparticles in toluene..

B-1-3 Environmental effect:

The synthesis of Pt or Pd NCs has been performed both in the presence and absence of hydrogen atmosphere under glove box with outgases solutions. In case of cobalt, due to its high sensitivity to oxygen, the synthesis is always performed in glove box with degassed solution.

Hydrogen is naturally produced by the chemical reduction. To perform the reaction under saturated H_2 atmosphere, a closed screw cap with three ports is used and the reducing and the capping agent are injected through a silicone septum (see figure 1B).

B-1-4 Case of bimetallic nanoparticle :

Similar procedure to the previous one is used to obtain the solution of metallic salt. As an example, in a typical experiment to obtain $Pt_{50}Pd_{50}$ from the solution of $PtCl_6(TDA)_2$ and $PdCl_4(TDA)_2$ in toluene 10 mL of platinum complex organic solution ($PtCl_6(TDA)_2$) and 10 ml of palladium complex organic solution ($PdCl_4(TDA)_2$) are added to 20 mL of toluene. In procedure I, 1.2 10^{-2} mol of octylamine (C_8NH_2) capping agent is added. Then the aqueous solution of reductant $NaBH_4$ (10 cm^3, 1 $mol.L^{-1}$) is introduced into the organic mixture with rapid stirring. In procedure II the reducing agent is added prior the capping agent with a ripening time τ_{rip} = 60 mn.

B-2 DFT calculation

The rPBE (revised Perdew-Becke-Erzernhof functional) has been used as implemented in the VASP code. [8,9] Projector augmented wave PAW pseudopotentials [10,11] represent the core electrons, whereas the valence electrons (Pt: 10; H: 1; N: 5; C: 4) are explicitly described by a plane-wave basis set (cutoff 400 eV). In order to investigate the shape of the platinum nanoparticles we assume that cubic NP exhibit (100) terminations, octahedral NP exhibit (111) terminations and truncated shapes exhibit both terminations. Then, calculating the relative stability of (100) and (111) slabs gives an indication of the particles morphology. The unit cells have been

chosen to have similar surface area and equal composition of the slab so the total energy can be easily compared. The (100) termination was modelled by a c2x2 unit cell (dimensions 5.635 × 5.635 × 35 $Å^3$) and the (111) termination by a 2x2 unit cell (dimensions 5.628 × 5.628 × 35 Å3), a vacuum of ~20 Å is included to prevent interaction between successive slabs. A 5×5×1 k-points scheme is used to sample the Brillouin zone. The thickness of the slabs is five atomic layers, each layer containing 4 Pt atoms (20 atoms per slab); the three uppermost layers are allowed to relax with the adsorbates, the two bottom layers were kept fixed to the ideal bulk positions. The ionic loop is converged below 1 meV using the conjugate gradient method. Dispersion forces have been included for all atoms in the slab, as implemented in the Grimme-D2 approach, the parameters used for Pt are C6= 19.46 Jnm^6mol^{-1}, R0 = 1.676 Å.

The reaction of adsorption of N molecules of type M on the slab (hydrogen or octylamine) is represented as: $$Slab + N•M = [Slab\text{-}NM] \quad (1)$$

The reaction energy associated to equation (1) can be used to estimate the stability of a slab from Gibbs free energies Gi and chemical potential μM:

$$\Delta Gr = G_{[Slab\text{-}NM]} - G_{slab} - N\mu_M \quad (2)$$

Neglecting volume and entropy changes because they are equal for the two slabs, the Gibbs energy can thus be replaced by the total-energy calculations as obtained from the calculations.

B-3 X-Ray scattering experiments and analysis

In situ SAXS experiments during nanoparticle growth were carried out on the SAXS station at SWING beamline of Soleil Synchrotron Radiation Facility (France). The incident X-ray energy was selected to be 11264eV (0.11nm in wavelength λ) for SAXS experiments by a double-crystal Si (111) monochromator below the Pt L_3 edge to avoid fluorescence effect. The scattering experiments were performed using a two-dimensional AVIEX CCD camera (170 x 170 mm^2, 4096 x 4096 pixels), moving in a vacuum detection tunnel in order to optimize the q range of scattering

patterns, where q is the scattering vector ($q = 4\pi\sin\theta/\lambda$, where θ is the scattering angle). Thus, the sample-detector distance was set to 1.2 m for SAXS measurement, given a q range between 0.01 and 8 nm^{-1}. The particle scattering signal was obtained after signal normalization by two ways: i) detector sensibility and incident beam ii) subtraction of the capillary-cell/pure-buffer-solution signal and air signal.

Particle size and shape analysis are complex to extract from SAXS pattern and typically requires fitting mathematical models of shape and of size distribution to the data. This method avoids approximations (e.g. Guinier gyration radius technique [12] or by applying some power law with the scattering vector q) commonly used to extract morphological parameters. We used a combination of fitting methods to extract particle dimensions (diameter D) and shape distribution from the SAXS data and cross-checking the methods against each other (TEM and HRTEM). We found, in general, good agreement between the results from SAXS and TEM data. [13]. The 1-D plot of X-ray scattering intensity patterns versus scattering vector, q, on a log–lin scale provides information about the nanoparticle morphology. The oscillations observed arise from the inherent form-factor scattering from the particles. These oscillations are often 'washed-out' by polydispersity in particle size or eventually in shape, requiring simulations with analytical models for the analysis. Because no interference maxima due to correlation between particles (small interparticle distance) were detected, we have considered data taken from the diluted samples. The scattered X-ray intensity becomes for an assembly of particles of a size distribution

$$N(R):\ I(\mathbf{q}) = \langle \Delta\rho \rangle^2 \int V^2(R) P(\mathbf{q},R) N(R) dR$$

with $P(\mathbf{q},R)$ is the form factor expression only dependent on the geometric shape of particles with $V(R)$ the volume of one single particle of an isotropic shape and $\Delta\rho$ the average scattering length density contrast. Quantitative data analyses of the SAXS patterns were performed using solid-sphere form factors

$$P_{sphere}(q,R) = 9\frac{(\sin(qR) - qr\cos(qR))^2}{(qR)^6}$$

In a first analysis and faceted shape form factors in a second step [14,15] with a Gaussian size distribution $N(R) = N/\sqrt{2\pi}\sigma\, e^{-\left[(R-R_0)^2/2\sigma^2\right]}$ where N, R_0 and σ are the density, the average radius and the radius standard deviation of particles. The electron density contrast between particles and the solution was only considered, assuming that the capping agent electron density is similar to the solution one with respect to the Pt one as in the case of gold studies [15].

C Result and Discussion

C-1 Pure Metallic Nanocrystals : influence of the metal on the size and shape

C-1-1 Platinum nanocrystals

It has been reported previously the effect of H_2 overpressure on the nanomorphology of platinum nanocrystals. [16] Pt nanoparticles obtained for capping agent added prior the reducing agent, (i.e procedure I) either in the absence or the presence of H_2 (see figure 1) are mostly spherical and characterized by a mean diameter of around 2 nm and a size dispersion of 18 %. (figure 2A). In both cases, HRTEM observations reveal well faceted and crystallized nanoparticles (figure 2B). This image exhibits mainly decahedral shape corresponding to a 5-fold symmetry polyhedron with the {111} facets, which is confirmed by the Fourier transform (figure 2C and 2D). In contrast, the synthesis performed by procedure II in the presence of an overpressure of H_2 (see figure 1B) leads to drastic changes of both size and shape of the nanoparticles (figure 2E). Indeed, 4.5 nm Pt nanocubes having 13% size dispersion are obtained in the presence of hydrogen while spherical and wormlikes particles are obtained in absence of H_2.[16,17] High resolution TEM (figure 2 F, G, H) shows also well crystallized nanoparticles where only {100} facets are exposed as deduced from the Fourrier transform of the HRTEM pictures (figure 2H). Thus the synthesis conditions, i.e.

the presence H_2 in the solution and the addition of the capping agent before or after the reduction influence strongly the platinum nanomorphology [17].

Shape control is often due to a specific poisoning of crystalline facets during the growth process. [2,18,19] In our case competition between amine and H_2 adsorption does change depending on the synthesis route. Hence, periodic DFT calculations have been carried out to compute the stability of the terminations of (111) and (100) slabs, the details of the calculations are given above. The bare (111)-terminated slabs are found to be more stable than the (100)-terminated ones in agreement with the literature [20] and thus in vacuum conditions octahedral or decahedral particles are expected to be formed. [21] As for the covered slabs, we have computed the interaction of dihydrogen, which is formed in the synthesis due to the addition of the reducing agent, and of the capping agent octylamine. It is known that H_2 dissociates without barrier at the platinum surfaces [22,23] therefore only atomic hydrogen adsorbed is considered: starting by 1, and increasing the H content up to 8 hydrogen atoms, all the compositions have been calculated. Hydrogen is found to adsorb on bridging sites for the (100) slab, and a mixture between bridge, top and hollow sites for the (111) slab, in agreement with previous calculations. [24] Table 1 shows the calculated adsorption energy for each slab. It is found that the (100) slab shows a higher affinity for adsorbing H, with exothermic E_{ads} per H between -0.70 eV (1H) to -0.56 eV (7H), whereas the (111) slab shows E_{ads} ranging between -0.58 eV (1H) to -0.51 eV (4H). Note that the maximum content of atomic hydrogen is 7H for (100) and 4H for (111), above these values atomic hydrogen recombines to form H_2 and desorbs. This behaviour confirms the higher affinity of (100) terminations for hydrogen compared to (111) termination. In order to investigate the role of the capping agent, the adsorption of octylamine is also computed and it is found to adsorb on top sites in both surfaces, tilted ~25 deg from the vertical of the slab. The calculated adsorption energies for the two slabs shown in Table 1 are very similar: -1.19 eV (111) and -1.23 eV (100), indicating that octylamine molecules have no preference for a given termination.

The shape of platinum nanoparticles can be qualitatively predicted based on the results presented above. The most exposed planes will be the most stable and will correspond to those growing more slowly. The ratio of the adsorption energies on each slabs, $E_{ads}(100)/(111)$ can be taken as a measure of the relative stability of the (100) slab with respect to (111): values higher than 1 indicate a stabilization of (100) termination and thus the particle tends to cubic shape; values lower than 1 indicate octahedral-shaped particles, and values close to 1 indicate that the two terminations are almost equivalent in energy and will expose the same area leading to truncated octahedral morphology. Our results explain the experimental procedure: the reducing agent must be introduced before the capping agent to stabilize (100) terminations. The further addition of octylamine will displace hydrogen stabilizing cubic shapes. Moreover, high pressure of hydrogen are needed, otherwise isotropic particles are obtained. This is obtained by using closed vessels. If the octylamine is added prior to the reducing agent, it will stabilize both (111) and (100) terminations. Due to the affinity of the octylamine for platinum it probably blocks the surface sites making the growth dynamic slower, leading to small isotropic particles.

C-1-2 Palladium nanocrystals

Palladium nanocrystals have been synthesised following the same process in presence of an overpressure of H_2 either in procedure I (figure 3A,B) or in (procedure II, (figure 3C,D). Conversely to the platinum case, there is no drastic change in the size and morphology of the palladium nanocrystals. However the shape appears more regular when synthesized following procedure I compare to procedure II. This could be due to a poorly crystalline structure of the seeds, which prevent the good anchoring of the capping agent on specific facets (figure 3D and inset figure 4D). In case of the palladium, it seems to be the major effect, as whatever are the synthetic procedure wormlike nanoparticles are obtained. Coming back to the chemical synthesis, H_2 is produced during the chemical reduction of metallic ions by $NaBH_4$. At room temperature and

at atmospheric pressure, hydrogen gas spontaneously adsorbs to Pd metal as atomic hydrogen and diffuses into the lattice to form PdHx, [25], which in turn change the physical properties of the palladium. [26] This probably induces a change in the growth process of Pd nanoparticles compare to Pt, as in case of weakly bonded capping agent as amine, whatever the synthesis procedure, H_2 can penetrate in the sublayer of the Pd nanocrystals to form palladium hydrides yielding to an amorphous surface and a lower interaction of the amino group of the capping agent with the palladium surfaces. [27] This is clearly evidenced by HR-TEM investigation (inset figure 4D) where the seed observed just before the addition of the capping agent appears poorly crystallized with amorphous surface. This is also observed on the passivate nanocrystals extracted and dispersed in toluene after the synthesis (figure 3B,D). Thus whatever the synthesis procedure, same nanoparticles are obtained due to the ability of H_2 to penetrate the passivating layer [25,27]: in the procedure I, the capping agent is added before the reducing agent, then the chemical reaction takes place with an overpressure of H_2, which could react with Pd to form PdH_x. In procedure II, as the reduction takes place with an overpressure of H_2, hence PdH_x is formed prior the addition of the capping agent. It is known that self-assembled monolayers could only be obtained on well-crystallized surfaces. Thus, in our case as the surface of nanoparticles is partly amorphous (see figure 3B,D and inset figure 4D), the capping layer should present numerous defects and/or its binding with the surface (hydride) differs from that of pure metal. As a consequence, the capping agent layer cannot protect efficiently from aggregation. This yields wormlike structures coexisting with spherical ones, whatever the synthetic procedure is. HR-TEM show also that the surface is more amorphous in case of procedure II (figure 3D) compare to procedure I (figure 3C), which could explain the large polydispersity in size and shape observed for palladium NCs synthesized by procedure II. This process is very different from the behaviour of platinum where H_2 is dissociated on platinum and adsorbed on the surfaces and could escape from the surfaces if the

tube is opened. It is the reason why it is necessary to maintain an overpressure of H_2 to obtain the platinum nanocubes (see experimental part).

C-2 Kinetics *in situ* investigation of the growth process of pure metallic nanoparticles.

In complement of the TEM investigation and DFT calculation and in order to give quantitative and qualitative response, growth evolution of platinum nanocrystals has been investigated in situ and in real time. We focus here on the complete description of the formation mechanism, which would require measuring the morphological evolution (i.e. size, shape and polydispersity) of nanoparticles with time. In this respect, Small Angle X-Ray Scattering (SAXS) is perfectly suited for assessing the particle growth kinetics in terms of nanomorphology [28-32]. Here, we have developed in situ SAXS investigations. A quantitative fitting of the scattering diagram allowed to determine the size distribution and the shape distribution of the first stage of nanoparticle formation and to follow their subsequent growth. The in situ investigation by SAXS is reported for both sample Platinum (obtained from procedure II, in the presence of an overpressure of H_2, figure 4B) and Palladium nanoparticles (obtained from procedure II, either in the presence, figure 4E or in absence of an overpressure of H_2, figure 4F) after a ripening time of 60 min. These measurements are made on small aliquots taking off directly in the chemical bath at a specific time after adding of the capping agent, from 0 to 16 hours. It is clear that the behavior totally differs. In the case of platinum nanocrystals obtained under H_2 overpressure, the SAXS patterns (figure 4B) show an evolution of the I (q) vs q curve with more and more pronounced oscillations and with a shorter period, characteristic of a progressive formation of low polydisperse isotropic nanostructures [33-36] of increasing size. Finally platinum nanocubes are obtained due to the H poisoning of the (100) facets (figure 4A). The average radius of nanocrystals was extracted from the adjustment of the experimental SAXS pattern by a simulation using a simple spherical form factor of particles (Figure 4C) and taking into account a size dispersion effect (see experimental

section). Figure 4C shows the evolution of this radius with the ageing time. There is a monotonic increase of the average size during the ageing process. Compare to the formation of nanocrystals in other liquid systems, the growth process is considerably slow down as it takes 16 hours while it takes a few second for reduction of gold in homogeneous solution [31, 37] or few minutes for silver in reverse micelles [38]. However, this evolution is consistent with a growth process based on the aggregation of the monomer (Pt^0) on the surface of the nuclei. In the liquid-liquid phase transfer synthesis developed by Brust et al. [7], it is assumed: i) the formation of monomer at the oil/water interface during the adding of the reducing agent, ii) transfer of the capped TDAB/monomer into the organic phase where the nucleation occurs, iii) growth process of the nuclei by aggregation of the monomer on the surface of the nuclei. The variation of the average radius in the time gives indication of the growth process and reactivity of the surfaces of the nuclei [15,31]. Here the average radius varies as $t^{1/2}$ (solid line on figure 4C). This indicates that the growth process is limited by the reactivity at the surface of the nuclei under a high overpressure of H_2 (i.e. t_0=60 min). [31].

This behaviour confirms the assumption of monomer's aggregation on the nuclei's surface [31] and not nuclei's aggregation. However, the presence of H, adsorbed at the platinum surface [22,23], strongly modified the kinetics of the growth process: for this sample, octylamine is added 60 mn after completion of the reduction (t_0=60 mn, i.e. with a high pressure of H_2 enough to passivate the platinum surface see above and [17]). This poisoning of the surface induces a slowdown of the aggregation process, as it is the incorporation of the monomer in the crystalline lattice of the nanoparticle, which is the limiting step of the growth process. This yields to larger nanocrystals as there is an accumulation of monomer close to the surface of the nanocrystals. This is reinforced because the interaction between octylamine and metal particle, which limits the final size, is lower in procedure II due to the H adsorption on the platinum surface (see above). Hence, we experimentally confirm the growth process assumed in the Brust synthesis [7] and it is clearly

demonstrates the effect of H_2 on the kinetic control of the nanocrystals size as predicted by the DFT calculation.

In case of palladium nanocrystals obtained by procedure II in the presence of an overpressure of H_2, a very different scattering pattern is obtained (figure 4E). There is no significant evolution of the SAXS pattern shape with the ageing time (the change of the intensity between 1 $nm^{-1} < q < 6$ nm^{-1} is only due to a variation of the amount of palladium nanocrystals in the aliquots studied as some inhomogeneity occurs during the reaction progress). In particular, there is no specific oscillation in a shorter time in the I(q) vs q curves characteristic of a particle with a specific shape growing by aggregation. However, at a very low angle, below 1 nm^{-1}, a strong increase of the scattered intensity is observed (where I(q) is proportional to q^{-1}), characteristic of the presence of elongated nanoparticles [33,35]. These results are in agreement with TEM observation (figure 4D) that clearly shown highly polydisperse spherical nanoparticles or nanowires. It should be noticed that this growth process is a consequence of the use of physisorbed octylamine passivating agent, which allows direct contact between the metal surfaces of the palladium nanocrystals and then the crystallographic reconstruction yielding to the nanowires. As expected from the model discussed above, there is no specific effect of the environment as the interaction of H_2 with the Pd surfaces yields to PdH_x in the presence or in the absence of an overpressure of H_2. Thus similar scattering patterns are obtained for palladium nanocrystals synthesized by procedure II but without maintaining an overpressure of H_2 (see figure 1A) after the capping agent addition (i.e. in open air figure 4F). Again the SAXS patterns show a homogenous evolution with time not observed in case of procedure II, which indicates a homogenous growth process, which could explain the better shape control in case of palladium, where the polydispersity is lower than that observed for palladium NCs obtained by procedure II. This reflects the strong influence of the anchoring of the capping agent on the growth process and finally on the shape control. [2,3]

Thus, as the shape control and the growth process in liquid−liquid phase transfer synthesis is strongly dependent on the binding of the capping agent on the metallic surfaces, we demonstrate here, with platinum and palladium, different behaviour due to a change of the metal surface state induced by the nature of the interaction of H_2 with the metal. Hence it is demonstrated that the chemical route and the nature of the metal strongly influence the shape and size of the metallic nanocrystals.

C-3 Platinum Derivated Nanoalloys.

The liquid-liquid phase transfer method presented above has been used to form either Co_xPt_{1-x} or Pd_xPt_{1-x} nanoalloys. Only a few works deal on nanoalloys obtained by this two-phase synthesis due to the difficulty to control their composition. We report previously the case of CoPt synthesis [39,40]. Perfect control on the composition can be only achieved if the two precursors are similar in structure and in location in the liquid media. As a matter of fact, the large difference in reduction potential of platinum (E_{SHE} Pt(II)/Pt = 1.2V) and cobalt (E_{SHE} Co(II)/Co = -0,28V) can induce a strong variation in the reduction kinetics. As an example, if platinum precursor is in the organic phase (complexed by the transfer agent) and the cobalt precursor in the water phase (as an aqueous salt), the reduction takes place during the emulsification of the solution obtained by stirring when the reducing agent is added. If the reduction of platinum is dominated by the interface, the reduction of cobalt is dominated by the reduction kinetics of the salt in the aqueous phase. Thus, the co-reduction is carried out in two distinct ways. Therefore, a strong discrepancy occurs in the average content of the cobalt in the nanocrystal compared to the expected ratio. Due to the change in the characteristics of the emulsion droplets from one to another, the homogeneity in composition is low. Conversely if both cobalt and platinum salts are in the organic phase interacting with an interface, only the reaction conditions are predominant and the difference in redox potentials is no longer a problem for this interfacial reaction [40]. Thus, the best results are

obtained when cobalt is in the same form as the platinum: $CoCl_2(TDA)_2$ and $PtCl_4(TDA)_2$, i.e. both complexed by the same agent transfer (see figure 5A). These two molecules have a similar structure and then the composition of the interface where the reduction takes place is directly related to the initial composition of metallic precursor. Hence, the reduction yields to a precise control of the composition.

C-3-1: *Nanoalloys obtained by adding capping agent prior the reducing agent (Procedure1)*

The same procedure as pure platinum or pure palladium has been used to attempt the formation of platinum based nanoalloys (see figure 5). The colloidal synthetic route used in this study enables us to prepare samples of $Co_{50}Pt_{50}$ NCs 2 nm in size (figure 5A). These crystals are quasi-spherical and have a homogeneous size with a polydispersity of 12%, which was determined from measurements of TEM images. The EDX analyser of a JEOL 5510LV Scanning Electron Microscope (SEM) was used to determine the average composition of the $Co_{50}Pt_{50}$ nanocrystals. [40] A thin film made up of nanocrystals was obtained by evaporation of a concentrated nanocrystal solution on silicon wafers at room temperature. The resulting film was thicker than 10 µm. In the case of EDX analysis (SEM), a 1-µm thickness is required to obtain a reliable analysis. Several areas of the film were measured and EDX spectra were treated by the ZAF analysis technique. (figure 5B). **It has been previously reported that these CoPt nanoparticles are well faceted and crystallized. [39] The 2nm in size exhibits either decahedral shape corresponding to a 5-fold symmetry polyhedron with the {111} facets, or truncated octahedron, which is an equilibrium shape of the fcc crystal.**

Similar procedure has been adapted to the case of Pt_xPd_{1-x} nanocrystals. Figure 5C and 5D shows typical result for $Pd_{50}Pt_{50}$. Again nanocrystals are spherical in shape with an average diameter of 2.2 nm and a low polydisperisty in size and composition. The average composition as determined by EDX analysis is maintained at 50/50 +/- 2%. To confirm the formation of PdPt alloys,

nanocrystals have been synthesized with various compositions by adjusting the initial metallic salts ratio in the synthesis (see method above). Figure 6 shows the TEM and HRTEM investigation for Pt_xPd_{1-x} nanocrystals depending on the composition. It can be noticed that the nanocrystals are homogeneous in size, shape and electronic contrast, which is consistent with formation of nanoalloys. [39,40] The as-prepared Pt_xPd_{1-x} nanoparticles have high crystallinity as evidenced by clearly resolved lattice fringes in HRTEM (figure 6) whatever the composition. It is known that PtPd bulk alloys form a complete solid solution [42], as their lattice parameters are very close (a_{Pt} = 0.392 nm and a_{Pd} = 0.389 nm for a similar fcc structure). Therefore the inter-lattice distance should not vary between Pd (111) *fcc* and Pt (111) *fcc*. From the HRTEM pictures and the FFT associated, the lattice parameter of the fcc structure is estimated to be 0.38 +/- 0.01 nm for all the composition. The constant stoichiometry observed for each composition, as well as the TEM and HRTEM results, rules out the possibility of nano-phase segregation or core-shell formation. As for CoPt, [39], both decahedron or truncated octatedron are observed. The structural investigation is in agreement with the formation of Pd_xPt_{1-x} nanoalloys in the disordered A_1 phase as indicated by the FFT, which is characteristic of fcc nanoalloys (figure 6).

It should be noticed that in both cases, nanoalloys could be easily obtained in a large range of composition depicted the difference of lattice parameters for Co and Pd compare to palladium. The mismatch is below 1% for Pt and Pd, when it is 10 % for Co and Pt (a_{Co} = 0.355 nm for *fcc* structure). This is consistent with a random substitution of platinum atom by cobalt or palladium atom in the platinum lattice. Indeed, our procedure allows a complete and precise control of the composition over a large range for both Co_xPt_{1-x} and Pd_xPt_{1-x} and could probably be extended to other type of bimetallic nanoparticles.

C-3-2: *Nanoalloys obtained by adding reducing agent prior the capping agent (Procedure 2)*

We have seen before that introducing the reducing agent prior the capping agent yield to the shape and size control of the pure metallic nanocrystals. It is however strongly dependant on the nature of the metal, hence what happened in the case of platinum derivate nanoalloys?

Figure 7 summarizes the result obtained by TEM investigation for both PdPt (figure 7A, B, and C) and CoPt (figure 7D,E, and F) if the reducing agent is added before the introduction of the capping agent (procedure II see figure 1). Starting from conditions where platinum nanocubes are obtained (figure 7A) it is not possible, by this chemical method, to control both the composition and the shape even in case of PtPd where a total solid solution exist in bulk materials. [42] For $Pt_{80}Pd_{20}$, well faceted cubo-octahedrons are obtained (figure 7B), which shows the persistent influence of hydrogen-platinum (which is the main component) interaction. This shape control totally disappears if the amount of palladium increases. Furthermore, it has not been possible to obtain stable nanocrystals starting from an equimolar solution of platinum and palladium salt: the NCs are probably too small to be recovered after the extraction process. Increasing the palladium content allows for stable NCs only for high palladium content (higher than 80%) but in this condition highly polydisperse NCs similar to those obtained for pure palladium (figure 7C) are obtained. Thus, only nanoalloys rich in palladium or rich in platinum could be obtained by this procedure. The situation appears more dramatic in the case of CoPt (figure 7D, E and F). By procedure II it is not possible to obtain nanoalloys. In fact at high content of cobalt, segregation occurs where both cobalt NCs, poorly crystallized, and small spherical platinum NCs are obtained (figure 7E). Decreasing the amount of cobalt (<50%) yields to small spherical NCs with an average composition of about 20 % of cobalt (as determined by EDX analysis). It should be noticed that pure Cobalt NCs could be obtained (figure 7F), however they are amorphous, unshaped and strongly oxidizible as amine cannot efficiently protect the cobalt surfaces. These results illustrate the importance of the complexation of the monomer by the capping agent to obtain a perfect

control of the composition. In our synthesis, nanoalloys can only be obtained with a large composition control following the procedure I, where the capping agent is added before the reducing agent. It is probably due to the fact that a stable composition of the interface during the reduction could only takes place in the presence of the passivating agent. As mentioned above, this probably reflects the difference in the kinetics of formation of Pt(0) and Pd(0) or Co(0) starting from metallic salt. It is known that generally the reduction rates correlate with reduction potentials. In case of palladium and platinum reduction potential are closer than in the case of cobalt and platinum (E_{SHE} Pt(II)/Pt = 1.2V ; E_{SHE} Co(II)/Co = -0,28V; E_{SHE} Pd(II)/Pd = 0.99 V). Thus a partial solid solution could be obtained in case of PdPt synthesized by procedure II when it is not possible in case of CoPt. This could also be due to the difference between the stability of the initial nuclei composed either of pure platinum or both cobalt and platinum or palladium and platinum. [43] Both effects can be corrected by complexation with the capping agent. This is the reason why, depicted the close vicinity of the lattice parameters (see above), it is easier to synthesize nanoalloys by adding capping agent prior to the reducing agent (procedure I) than the opposite (procedure II).

D-Conclusion

Platinum and Palladium nanocrystals can be easily obtained by wet chemistry in ambient conditions using metallic salt as precursor. These materials have diverse applications in chemistry and physics. Control of the shape of the pure metal NCs or Platinum based nanoalloys can be very useful to reach new properties for catalysis or magnetic data storage, but the control of both the composition and shape is always a challenge. Indeed as reported here, this is strongly metal dependant and numerous parameters have to be taken into account in order to understand and to control the chemical process. We have shown here the role of the dissolved gases and on the capping agent. This study shows us that it is necessary for future development to design the

precursor in order to tune the reduction potential and thus the reduction rates of the metallic salt but also the state of the metallic surfaces of the growing seed in order to obtain nanoalloys with both specific composition and shape.

Aknowledgements

This work was supported by the French ANR within the programme "Nanocrisnet" under reference ANR-11-BS10-018. We thank SOLEIL for having provided the installations in synchrotron as well as Dr. Franck Meneau for the help brought for the use of the line of light "SWING ". Calculations was performed using HPC resources from GENCI- CINES/IDRIS (grants x2011082131, x2012082131, and x2013082131 for 2011− 2013, respectively) and the CCRE-DSI of the University P. M. Curie. Thanks to SMART-IP2CT (FR UPMC-CNRS 2622) for financial support.

E-References.

1- T.K, Kau, A.L., Rogach, F., Jäckel, , T.A., Klar, and J., Feldmann, *Advanced Materials,* 2009, 1, 21

2- G.J. Leong, M.C. Schulze, M.B. Strand, D. Maloney, S.L.Frisco, H.N. Dinh, B. Pivovar, and R.M Richards, *Applied Organometallic Chemistry*, 2014, 28, 1-17.

3- C., Petit, C., Salzemann and A., Demortière in "*Complex-shaped Metal Nanoparticles : Bottom-up Syntheses and Application*" Tapan K. Sau and Andrey, L. Rogach Editors, Wiley-VCH (2012)

4- Q, Zhang, J., Xie, Y., Yu, J.Y., Lee, *Nanoscale* , 2010, 2, 1962.

5- J., Park, J., Joo, S.G., Kwon, Y., Jang, T. Hyeon, *Angewandte Chemie,* 2007, 46, 4630.

6- J., Turkevich, P., Stevenson, C., Hilier, *J., Discuss. Faraday Soc.* 1951, 11, 55.

7- M., Brust, M., Walker, D., Bethell, D. J., Schiffrin, and R., Whyman, *J. Chem. Soc., Chem. Commun*., 1994, *7*, 801-802.

8- G., Kresse, J., Hafner, *Phys. Rev. B* 1993, 47, 558.

9- G., Kresse, J., Hafner, *Phys. Rev. B* 1994, 49, 14251.

10- P. E., Blochl, *Phys. Rev. B* 1994, 50, 17953-17979.

11- G., Kresse, D., Joubert, *Phys. Rev. B* 1999, 59, 1758-1775.

12- A., Guinier, G., Fournet *Small-Angle Scattering of X-rays* (Wiley, New York, 1955)

13- P., Andreazza in "*Nanoalloys*", Ed. D. alloyeau, C. Mottet, C. Ricolleau, (Springer Eds, 2012) 69-112

14- S., Disch, E., Wetterskog, R. P., Hermann , G., Salazar-Alvarez, P., Busch, T., Brückel, L., Bergström and S., Kamali *Nano Letters* 2011, 11, 1651-1656

15- S., Gómez-Graña, F., Hubert, F., Testard, A., Guerrero-Martínez, I., Grillo, L.M., Liz-Marzán and O , Spalla *Langmuir*, 2012, 28, 1453–1459

16- a- A., Demortières P., Launois N., Goubet P.-A., Albouy and C., Petit *J. Phys. Chem B,* 2008, 112, 14583.; b- C., Salzemann and C., Petit *Langmuir*, 2012, 28, 4835-4841.

17- N., Aguilera-Porta, M., Calatayud, C., Salzemann and C., Petit *J.Phys. Chem C*, 2014, 118, 9290−9298

18- "Complex-shaped Metal Nanoparticles : Bottom-up Syntheses and Application" Tapan K. Sau and Andrey, L. Rogach Editors , Wiley-VCH (2012) and reference therein.

19- Y., Xia, Y., Xiong, B., Lim, S. E., Skrabalak, *Angewandte Chem. Int. Ed.* 2009, 48, 60-103.

20- L., Vitos, A. V.;,H. L.;,Ruban, Skriver, J., Kollar, *Surf. Sci.* 1998, 411, 186–202.

21- F., Baletto, R., Ferrando, A., Fortunelli, F., Montanelli and C., Mottet, J. Chem. Phys. 202,116,3856-3863.

22- A. C., Luntz, J. K., Brown, M. D., Williams. *J. Chem. Phys.* 1990, 93, 5240-5246.

23- R. A., Olsen, G. J., Kroes, E. J., Baerends, *J. Chem. Phys.* 1999, 111, 11155-11163

24- D. C., Ford, Y., Xu, M., Mavrikakis, *Surf. Sci.* 2005, 587, 159-174.

25- M., Johansson, E. Skúlason , G. Nielsen, S. Murphy, R.M. Nielsen, I. Chorkendorff, *Surface Science* 2010, 604, 718–729

26- A., Henglein, *J.Phys.Chem.B.,* 2000, 104, 6683

27- F. J., Ibanes, F.P., Zamborini, J. *Am. Chem. Soc.,* 2000, 130, 622.

28- W., Wang, X., Chen, Q., Cai, G., Mo, L., Jiang, K., Zhang, Z., Chen, Z. Wu, and W., Pan, *Eur. Phy. J. B* 2008 , 65, 57-64.

29- H. G., Alison, R. J., Davey, J., Garside, M. J., Quale, G. J. T., Tiddy, D. T. Clarke and G. R., Jones, *Phys. Chem. Chem. Phys.,* 2003, 5, 4998–5000

30- M., Mougenot , P., Andreazza, C., Andreazza-Vignolle, R., Th., Escalier Sauvage, O., Lyon, P., J. Brault *Nanopart. Research,* 2011,14, 672.

31- B., Abecassis, F., Testard, O., Spalla, P., Barboux, *Nano Lett.* 2007, 7, 1723.

32- H.K., Kammler, G., Beaucage, D., Kohls, N., Agashe, J., Ilavsky *J. Appl. Phys.* 2005, 97, 054309.

33- Neutrons, X-Rays and Light:, Scattering Methods Applied to Soft Condensed Matter, P. Lindner and Th. Zemb eds., (North Holland, Amsterdam, 2002.)

34- O.;,Glatter, O., Kratky, Small Angle X-ray Scattering; Academic, Press: London, 1982.

35- C., Petit P., Lixon and M.P., Pileni *Langmuir* 1991, 7, 2620.

36- I. Lisiecki, P., André, A., Filankembo, C., Petit, J., Tanori, T., Gulik-Krzywicki, B.W., Ninham, M.P., Pileni, *J.Phys. Chem ;* 1999, 103, 9168.

37- N. R., Jana, L., Gearheart, C. J. Murphy, *Adv. Mater.* 2001, 13, 1389-1393

38- C., Petit, P. Lixon and M.P., Pileni; *J. Phys. Chem*. 1990, 94, 1598.

39- A., Demortière, C. Petit, Langmuir, 2007, 23, 8575.

40- A., Demortière, R., Losno, C Petit,.and J.P., Quisefit, *Anal. Bioanal. Chem.* 2010, 397, 1485.

41- Y. Cheng, and D.J., Schiffrin, *J Chem. Soc., Faraday Trans.* 1996, 92, 3865.

42- L., Bindi, F., Zaccari, G., Garutti,and N. Avigli, *Mineralogical Magazine* 2013, 77, 269-274.

43- R. Ferrando, J. Jellineck, R.L. Johnston, Chem Rev, 2008 108, 845

Table 1: calculated adsorption energy for the hydrogenated and octylamine covered slabs, in eV, calculated as $E_{ads} = (E_{NM} - E_{slab} - NE_M)/N$ where M is $1/2H_2$ or C_8NH_2 molecule calculated in the gas phase, and E_{slab} refers to the reference energy for each slab. $E_{ads}(100)/(111)$ measures the relative stability of the two terminations: values > 1 indicate predominance of cubic, values < 1 indicate predominance of octahedral particles.

	E_{ads} (111)	E_{ads} (100)	$E_{ads}(100)/(111)$ (predicted shape)
0H	-118.85*	-116.72*	0.982 (truncated octahedron)
1H	-0.58	-0.70	1.22 (cubic)
2H	-0.55	-0.70	1.27 (cubic)
3H	-0.44	-0.68	1.57 (cubic)
4H	-0.51	-0.72	1.43 (cubic)
5H	-0.39 [a]	-0.63	1.61 (cubic)
6H	-0.37 [a]	-0.54	1.47 (cubic)
7H	-0.31 [a]	-0.56	1.81 (cubic)
8H	-0.28 [a]	-0.49 [a]	1.75 (cubic)
C_8NH_2	-1.19	-1.23	1.03 (truncated octahedron)

[a] molecular H_2 is formed * total energy

Figure 1: Description of the two procedures used for the platinum synthesis: (A) in open air; (B) in a glovebox, under nitrogen flux. Two procedures are possible and are differentiated by the reduction done after (Procedure I) or before (Procedure II) the adding of the alkylamine.

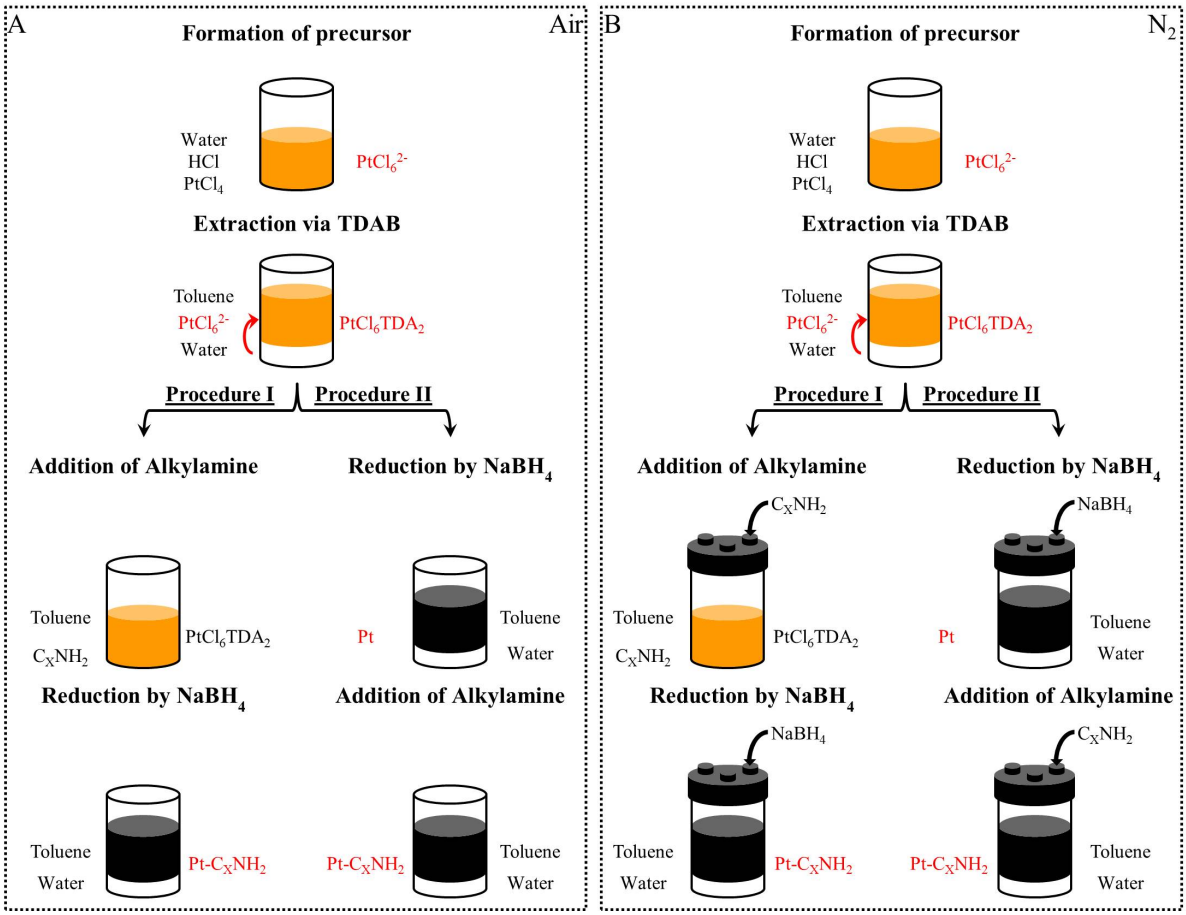

Figure 2: Pt-C_8NH_2 nanoparticles synthesized under overpressure of H_2 from procedure I : TEM image (A) and HRTEM images (B-C) with FFT associated (D) and from procédure II : TEM image (E) and HRTEM image (F-G) with FFT associated (H)

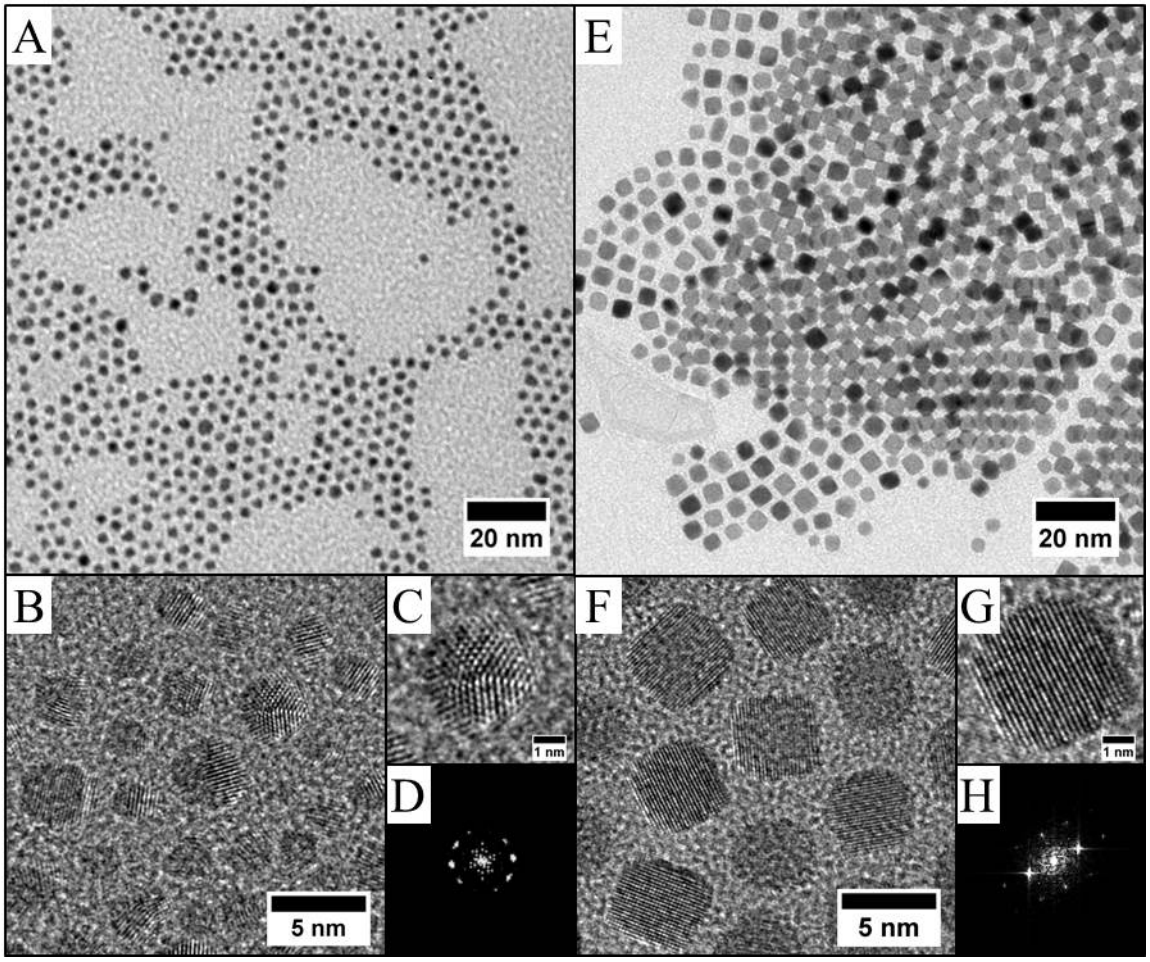

Figure 3: Pd-C_8NH_2 nanoparticles obtained under overpressure of H_2 from procedure I : TEM image (A) and HRTEM image (B) and from procedure II : TEM (C) and HRTEM (D) images.

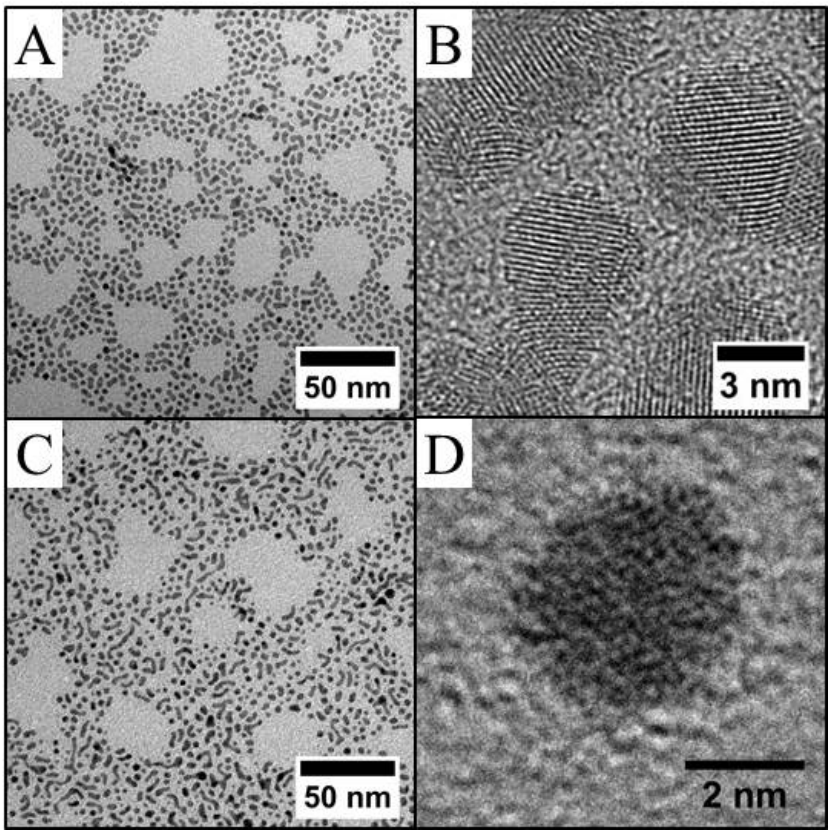

Figure 4: TEM image of Pt-C_8-NH_2 nanoparticles (A) and Pd-C_8-NH_2 nanoparticles (D) obtained via procedure II with an overpressure of H_2. SAXS patterns as a function of ageing time during the formation of (B) Pt nanoparticles after the ripening step, under hydrogen overpressure atmosphere (E) Pd nanoparticles after the ripening step, under hydrogen overpressure atmosphere. (F) Pd nanoparticles after the ripening step, without hydrogen overpressure atmosphere. Inset (D) HRTEM of Palladium seed before the addition of the capping agent. (C) Evolution of the average radius deduced from SAXS fitting with the ageing time (t_0= 60mn)

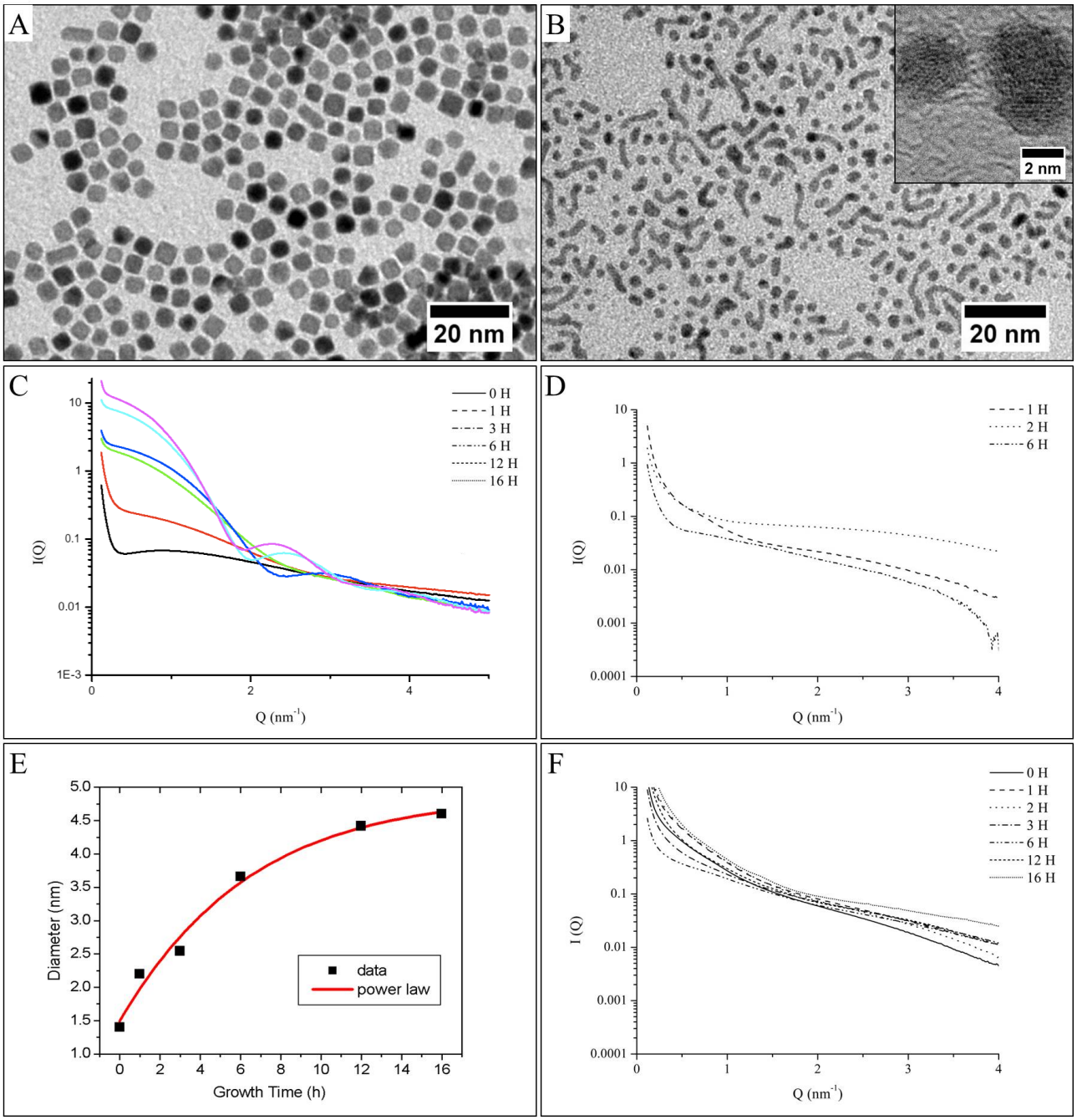

Figure 5: TEM images of CoPt-C_8NH_2 (A) and PdPt-C_8NH_2 (C) with their respective EDX analysis (B and D)

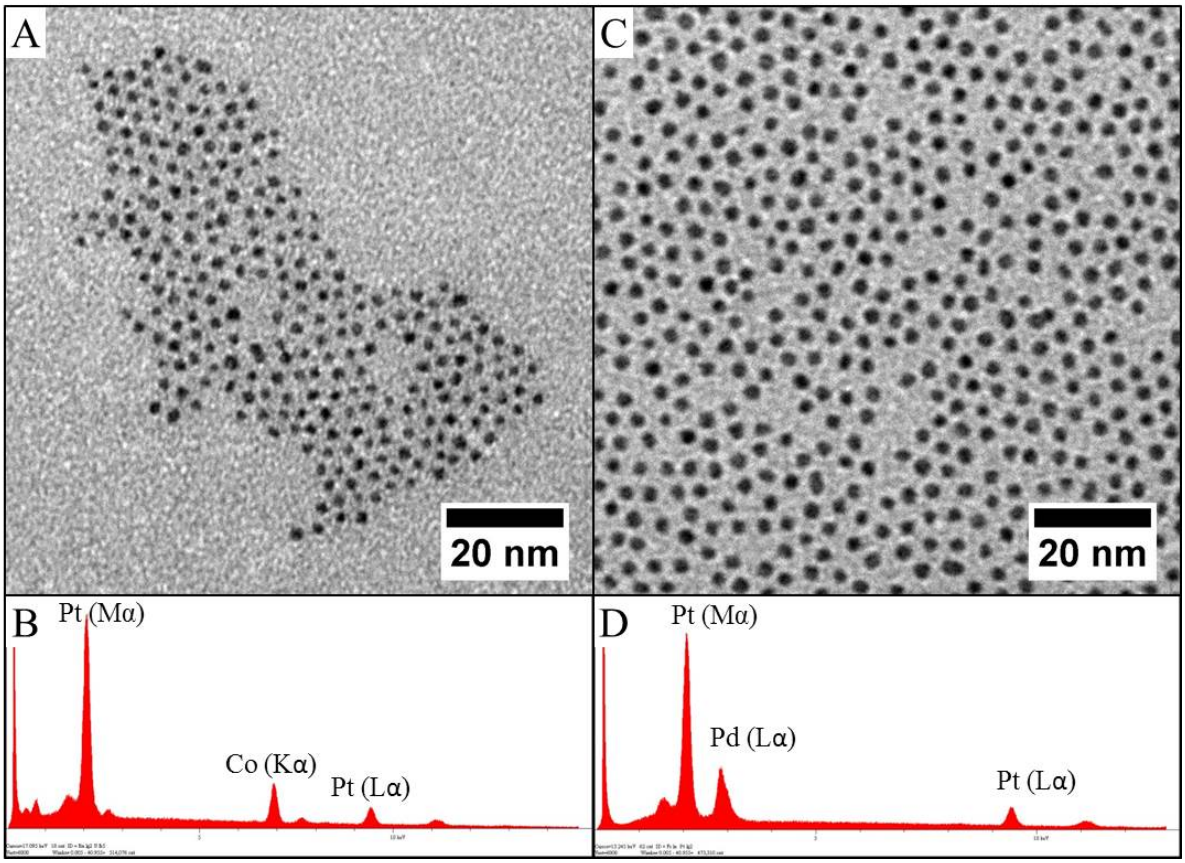

Figure 6: TEM image (1), HRTEM image (2) with a zoom on one nanoparticle (3) and associated FFT (4) of (A) Pd_0Pt_{100}-C_8NH_2, (B) $Pd_{20}Pt_{80}$-C_8NH2, (C) $Pd_{50}Pt_{50}$-C_8NH_2, (D) $Pd_{80}Pt_{20}$-C_8NH_2 and (E) $Pd_{100}Pt_0$-C_8NH_2. The different composition were obtained by adjusting salts volumic ratio

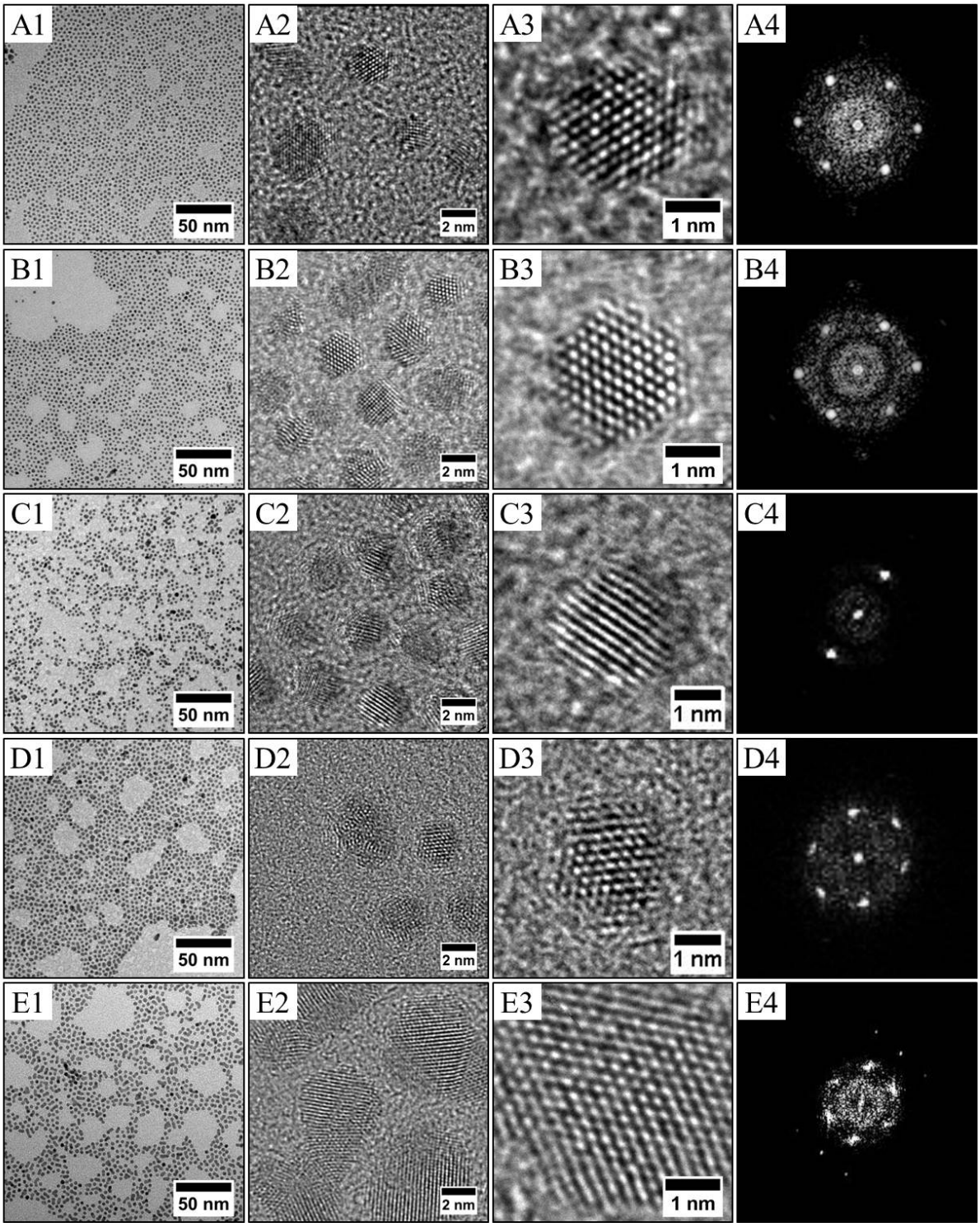

Figure 8: TEM images of Pd_XPt_{100-X}-C_8NH_2 with (A) X=0, (B) X = 20 and (C) X=100 obtained using procedure II with an overpressure of H_2; TEM images of Co_XPt_{100-X}-C_8NH_2 with (D) X=20, (E) X=80 and (F) X=100. The equiatomic compositions were not obtained.

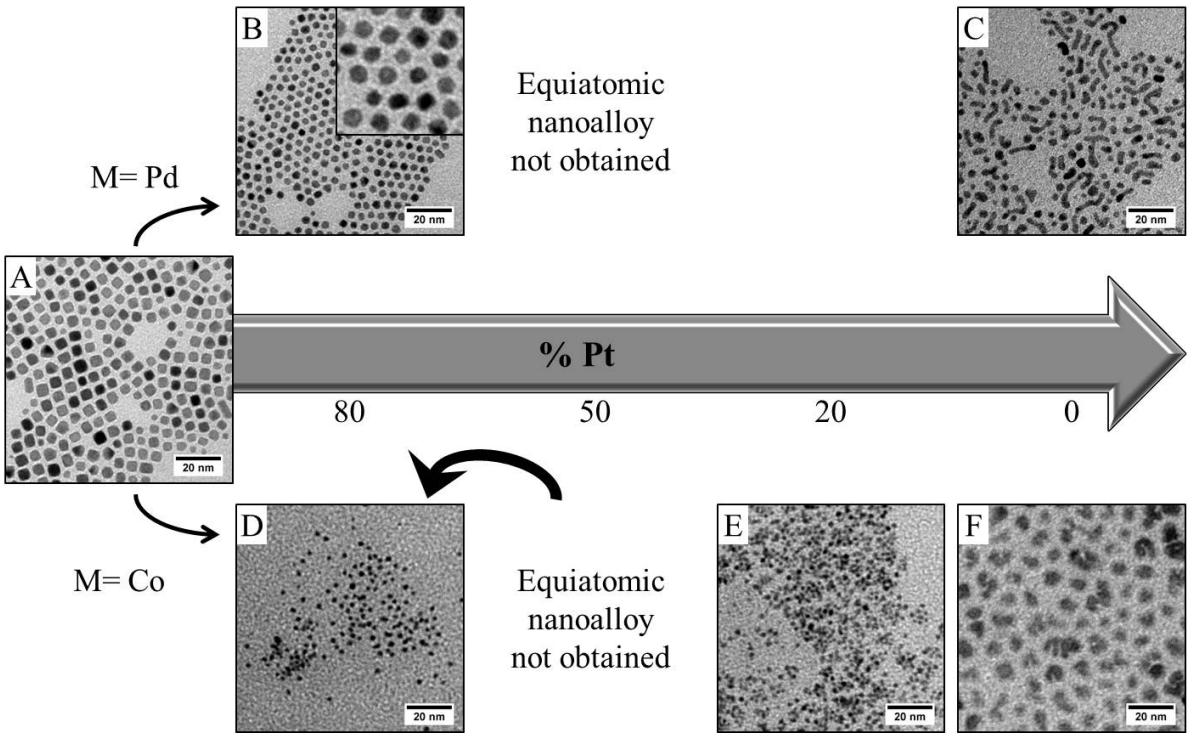

Figure 1: Description of the two procedures used for the platinum synthesis: (A) in open air; (B) in a glovebox, under nitrogen flux. Two procedures are possible and are differentiated by the reduction done after (Procedure I) or before (Procedure II) the adding of the alkylamine.

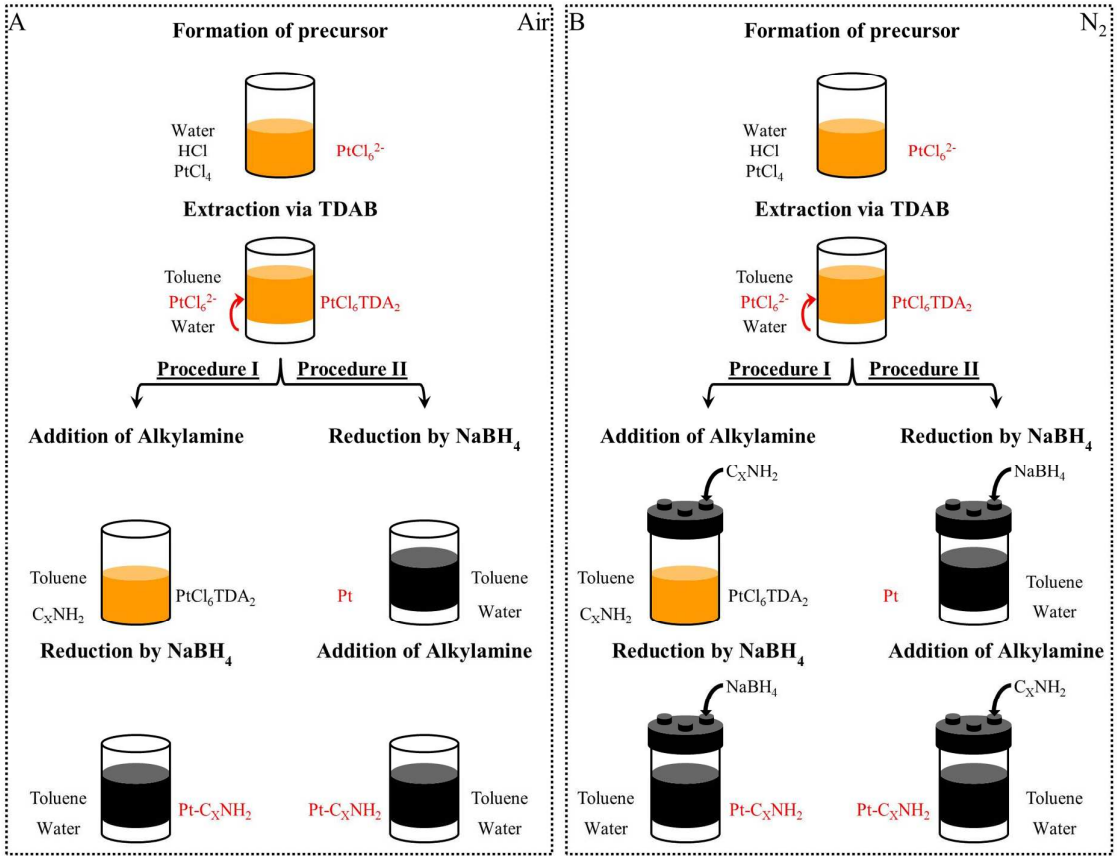

Figure 2: Pt-C_8NH_2 nanoparticles synthesized under overpressure of H_2 from procedure I : TEM image (A) and HRTEM images (B-C) with FFT associated (D) and from procedure II : TEM image (E) and HRTEM image (F-G) with FFT associated (H)

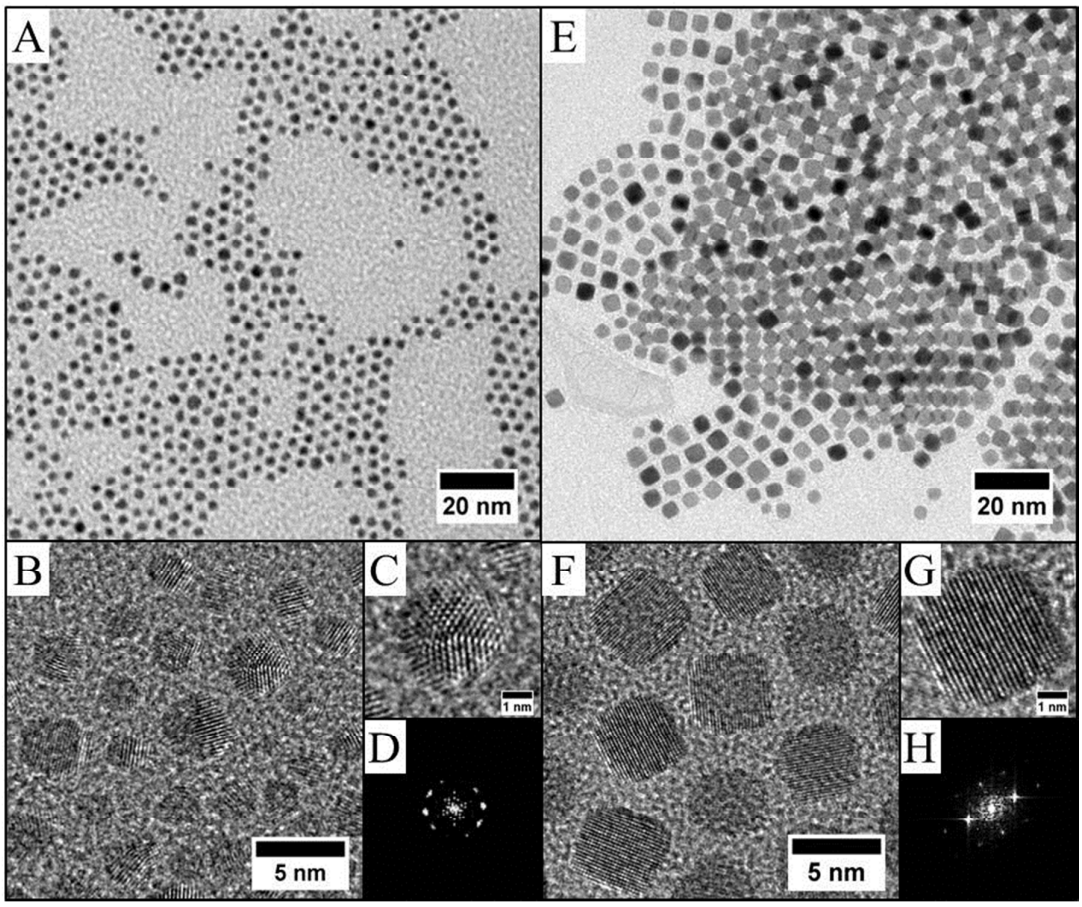

Figure 3: Pd-C_8NH_2 nanoparticles obtained under overpressure of H_2 from procedure I : TEM image (A) and HRTEM image (B) and from procedure II : TEM (C) and HRTEM (D) images.

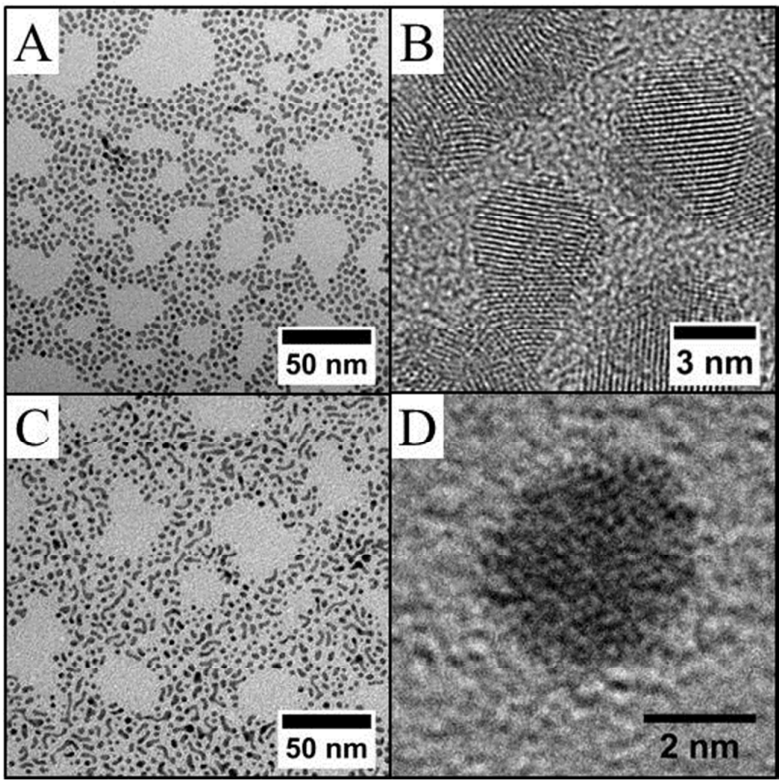

Figure 4: TEM image of Pt-C_8-NH_2 nanoparticles (A) and Pd-C_8-NH_2 nanoparticles (D) obtained via procedure II with an overpressure of H_2. SAXS patterns as a function of ageing time during the formation of (B) Pt nanoparticles after the ripening step, under hydrogen overpressure atmosphere (E) Pd nanoparticles after the ripening step, under hydrogen overpressure atmosphere. (F) Pd nanoparticles after the ripening step, without hydrogen overpressure atmosphere. Inset (D) HRTEM of Palladium seed before the addition of the capping agent. (C) Evolution of the average radius deduced from SAXS fitting with the ageing time (t_0= 60mn)

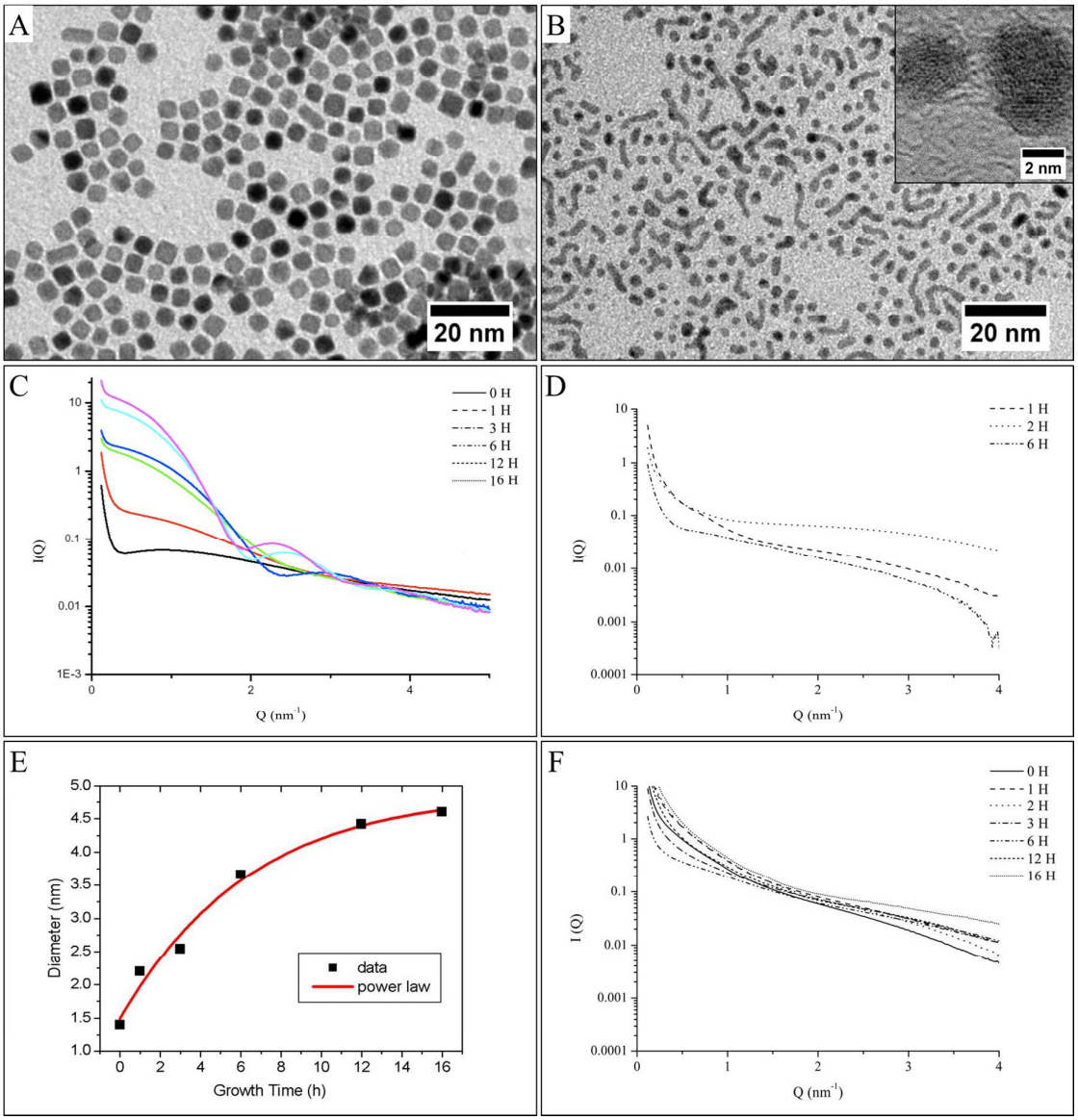

Figure 5: TEM images of CoPt-C_8NH_2 (A) and PdPt-C_8NH_2 (C) with their respective EDX analysis (B and D)

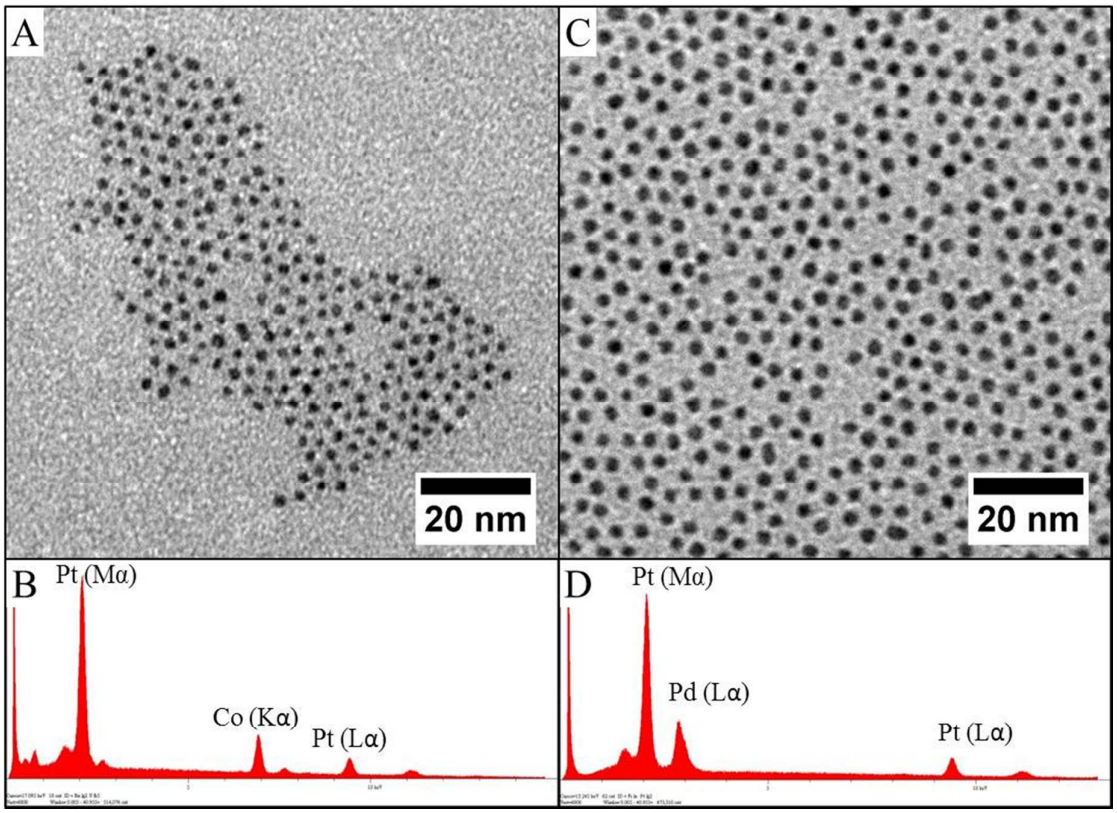

Figure 6: TEM image (1), HRTEM image (2) with a zoom on one nanoparticle (3) and associated FFT (4) of (A) Pd_0Pt_{100}-C_8NH_2, (B) $Pd_{20}Pt_{80}$-C_8NH_2, (C) $Pd_{50}Pt_{50}$-C_8NH_2, (D) $Pd_{80}Pt_{20}$-C_8NH_2 and (E) $Pd_{100}Pt_0$-C_8NH_2. The different composition were obtained by adjusting salts volumic ratio.

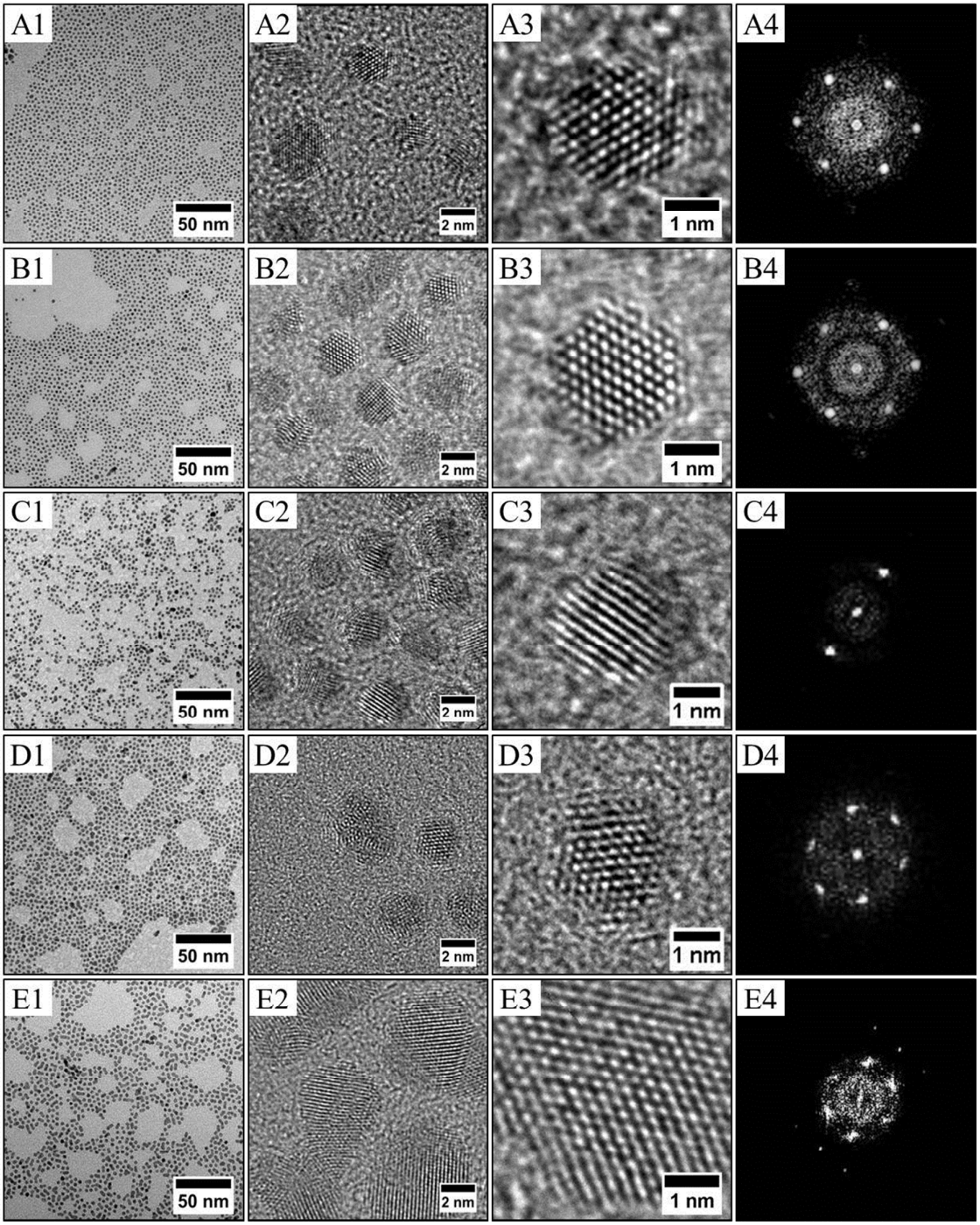

Figure 8: TEM images of Pd_XPt_{100-X}-C_8NH_2 with (A) X=0, (B) X = 20 and (C) X=100 obtained using procedure II with an overpressure of H_2; TEM images of Co_XPt_{100-X}-C_8NH_2 with (D) X=20, (E) X=80 and (F) X=100. The equiatomic compositions were not obtained.